

Microtubule cross-linking triggers the directional motility of kinesin-5

Lukas C. Kapitein,^{1,2,3} Benjamin H. Kwok,⁴ Joshua S. Weinger,⁴ Christoph F. Schmidt,^{1,2,5} Tarun M. Kapoor,⁴ and Erwin J.G. Peterman¹

¹Department of Physics and Astronomy and ²Laser Centre, Vrije Universiteit, 1081 HV Amsterdam, Netherlands

³Department of Neuroscience, Erasmus Medical Center, 3015 GE Rotterdam, Netherlands

⁴Laboratory of Chemistry and Cell Biology, The Rockefeller University, New York, NY 10021

⁵III. Physikalisches Institut, Fakultät für Physik, Georg-August-Universität, 37077 Göttingen, Germany

Although assembly of the mitotic spindle is known to be a precisely controlled process, regulation of the key motor proteins involved remains poorly understood. In eukaryotes, homotetrameric kinesin-5 motors are required for bipolar spindle formation. Eg5, the vertebrate kinesin-5, has two modes of motion: an adenosine triphosphate (ATP)-dependent directional mode and a diffusive mode that does not require ATP hydrolysis. We use single-molecule experiments to examine how the switching between these modes is controlled. We find that

Eg5 diffuses along individual microtubules without detectable directional bias at close to physiological ionic strength. Eg5's motility becomes directional when bound between two microtubules. Such activation through binding cargo, which, for Eg5, is a second microtubule, is analogous to known mechanisms for other kinesins. In the spindle, this might allow Eg5 to diffuse on single microtubules without hydrolyzing ATP until the motor is activated by binding to another microtubule. This mechanism would increase energy and filament cross-linking efficiency.

Introduction

During cell division, the bipolar mitotic spindle is assembled to orchestrate equal segregation of the genetic material into two daughter cells. Shape, size, and function of the mitotic spindle depend on the motile properties of microtubule-based motor proteins (Sharp et al., 2000; Wittmann et al., 2001). Eg5, an evolutionarily conserved member of the kinesin-5 family, plays a key role in organizing microtubules into a bipolar spindle (Sawin et al., 1992; Cole et al., 1994). The homotetrameric configuration of kinesin-5 is crucial for its *in vivo* function in budding yeast (Hildebrandt et al., 2006) and is arranged such that one pair of motor domains is located at each end of a central stalk (Kashina et al., 1996). Consistent with this structure, it has been demonstrated that Eg5 can cross-link two microtubules and slide them apart (Kapitein et al., 2005).

In earlier work, we have explored the motility characteristics of Eg5 using single-molecule fluorescence experiments

(Kwok et al., 2006). The movement of single homotetrameric Eg5 molecules includes an ATP hydrolysis-independent diffusive component in addition to directional processive runs. Similar 1D diffusion along microtubules has been found for other microtubule-based motor proteins and is believed to play functional roles in cells (Vale et al., 1989; Culver-Hanlon et al., 2006; Helenius et al., 2006).

It is also known that the ATPase cycle of kinesins is allosterically controlled by microtubule binding (Kuznetsov and Gelfand, 1986). This prevents unproductive ATP hydrolysis when the motor is not interacting with a microtubule. Furthermore, kinesin-1 switches from an inhibited, microtubule unbound state to a motile state upon cargo binding (Hackney et al., 1992; Stock et al., 1999). Thus, for kinesin-1, motor activity requires binding both a microtubule and cargo. For the homotetrameric Eg5, it turns out that microtubules are both track and cargo. Therefore, the motor would need to differentiate between interactions with one and two microtubules. Such a regulatory mechanism for Eg5 had not been identified.

L.C. Kapitein and B.H. Kwok contributed equally to this paper.

T.M. Kapoor and E.J.G. Peterman contributed equally to this paper.

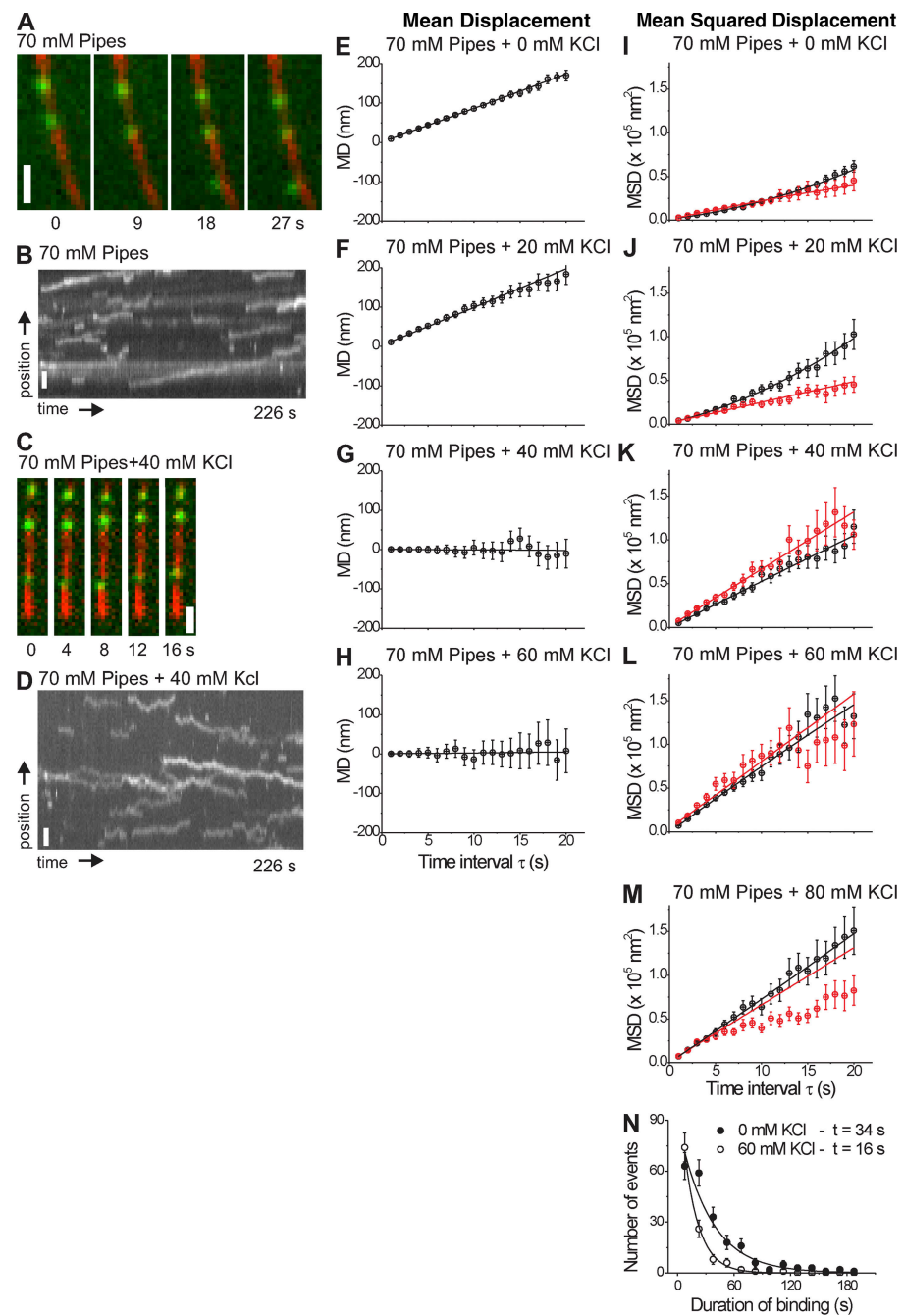
Correspondence to Christoph F. Schmidt: cfs@nat.vu.nl; or Tarun M. Kapoor: kapoor@mail.rockefeller.edu

Abbreviations used in this paper: MD, mean displacement; MSD, mean squared displacement; TIRF, total internal reflection fluorescence.

The online version of this article contains supplemental material.

© 2008 Kapitein et al. This article is distributed under the terms of an Attribution-Noncommercial-Share Alike-No Mirror Sites license for the first six months after the publication date (see <http://www.jcb.org/misc/terms.shtml>). After six months it is available under a Creative Commons License (Attribution-Noncommercial-Share Alike 3.0 Unported license, as described at <http://creativecommons.org/licenses/by-nc-sa/3.0/>).

Figure 1. Full-length Eg5 motility on single microtubules depends on ionic strength. (A and B) Frames (A) and kymograph (B) from a time-lapse recording showing single molecules of Eg5-GFP (green) moving directionally along a microtubule (red) in the presence of 70 mM Pipes. (C and D) Frames (C) and kymograph (D) from a time-lapse recording showing single molecules of Eg5-GFP (green) diffusing along a microtubule (red) in the presence of 70 mM Pipes plus 40 mM KCl. (E–H) MD calculated from Eg5-GFP motility in the presence of ATP (black) and ADP (red) in 70 mM Pipes plus 0, 20, 40, or 60 mM KCl. Fits represent $MD = v\tau$. (I–M) MSD calculated from Eg5-GFP motility in the presence of ATP (black) and ADP (red) and at the indicated ionic strengths. Fits represent $MD = v\tau$ and $MD = v^2\tau^2 + 2D\tau + \text{offset}$ for the ATP data and $MD = 2D\tau + \text{offset}$ for the ADP data. All numerical results are listed in Table I. (N) Histogram of the duration of binding events for 0 mM KCl and for 60 mM KCl added. Lines are single exponential fits ($\exp[-t/t_{av}]$) to the data (0 mM: $t_{av} = 34 \pm 3$, $n = 212$; 60 mM: $t_{av} = 16 \pm 2$, $n = 119$). Error bars represent SD. Bars, 1 μm .



Here, we have examined in single-molecule experiments whether Eg5 is regulated via switching between the directional and diffusive modes. We found that for full-length *Xenopus laevis* Eg5, diffusive and directional motility on single microtubules can be modulated by changing the ionic strength. Significantly, we found that at ionic strengths close to physiological conditions, full-length Eg5 diffused along single microtubules, whereas a dimeric construct did not show persistent microtubule interactions. Full-length Eg5 switched to directed motion when bound between two microtubules, resulting in relative sliding of microtubules. This suggests a track/cargo interaction-based regulatory mechanism that allows Eg5 to move processively only when cross-linking two microtubules.

Results and discussion

Eg5's motility on single microtubules switches from directional to diffusive upon increasing ionic strength

Ionic strength is known to influence motor–microtubule interactions (Okada and Hirokawa, 2000). To explore Eg5 regulation, we used *in vitro* single-molecule fluorescence motility assays to examine Eg5-GFP motility on individual microtubules in buffers with various ionic strengths. We found that in buffers with relatively low ionic strength (<100 mM potassium), motors moved unidirectionally toward one end of the microtubule with a speed of $\sim 10\text{--}15 \text{ nm/s}$, as we observed previously (Fig. 1, A and B; Kwok et al., 2006). In the presence of additional salt

Table I. Summary of speed and diffusion constants measured for kinesin-5 under different experimental conditions

Buffer (70 mM Pipes + KCl added)	ATP				ADP			
	MD		MSD		MSD		MSD	
	v (nm/s)	D ($\times 10^3$ nm 2 /s)	n	v (nm/s)	D ($\times 10^3$ nm 2 /s)	n	D ($\times 10^3$ nm 2 /s)	n
0 mM	8.9 ± 0.1	0.67 ± 0.02	77	9.1 ± 0.6	0.63 ± 0.06	77	1.06 ± 0.06	72
20 mM	10.1 ± 0.3	1.34 ± 0.04	62	11 ± 1	1.2 ± 0.2	62	1.18 ± 0.06	66
40 mM	0.0 ± 0.40	2.38 ± 0.07	50	0 ± 3 × 10 4	2.6 ± 0.2	81	3.3 ± 0.1	60
60 mM	0.3 ± 0.6	3.3 ± 0.1	48	0 ± 1 × 10 6	3.8 ± 0.3	123	3.8 ± 0.2	103
80 mM	ND	ND	NA	3.1 ± 8.1	3.6 ± 0.3	60	3.3 ± 0.3 ^o	90
60 mM (axonemes)	23.0 ± 0.4	2.39 ± 0.07	42	26.0 ± 1.3	1.8 ± 0.3	42	1.29 ± 0.09	54

NA, not applicable.

^oFit to first 5 s.

(20–50 mM KCl), Eg5-GFP motility appeared diffusive along the microtubule axis without clear directionality (Fig. 1, C and D). The fluorescence intensities of individual spots were similar under all conditions tested, demonstrating that the motors were in the same oligomeric state (unpublished data).

To systematically and quantitatively analyze the dependence of Eg5-GFP motility on ionic strength, we kept buffer concentration and pH constant (70 mM Pipes, pH 6.8) and added increasing amounts of KCl. For each buffer condition, >60 trajectories of individual Eg5-GFP tetramers were extracted from the recordings, and both the mean squared displacement (MSD) and the mean displacement (MD) were calculated for increasing time intervals, τ (Fig. 1, E–M; Kwok et al., 2006). The velocities and diffusion constants obtained from a second-order polynomial fit to $MSD(\tau)$ and from linear fits to $MD(\tau)$ and to the variance of the $MD(\tau)$ are summarized in Table I. The 1D diffusion constant increased with increasing salt concentration (from $D = 0.63 \pm 0.06 \times 10^3$ nm 2 /s at 0 mM KCl to $D = 3.6 \pm 0.3 \times 10^3$ nm 2 /s at 80 mM KCl), whereas the mean velocity dropped (from ~10 nm/s at low salt to 0 nm/s at higher salt concentrations). Furthermore, we found that the average duration of motile events decreased from 34 ± 3 s with no KCl added to 16 ± 2 s in the presence of an additional 60 mM KCl (Fig. 1 N). These results show that upon addition of more salt, Eg5-GFP's motility changed from a combination of directional motion and diffusion (<20 mM KCl) to purely diffusive motion (>40 mM KCl). The exact ratio of diffusive and

directional motion depends on ionic strength, with diffusive motion predominating under close to physiological conditions.

We previously showed that diffusive motion of Eg5-GFP on microtubules did not require ATP hydrolysis, and, in the presence of ADP, only the diffusive mode of motion was observed (Kwok et al., 2006). Here, we found that the dependence of the diffusion constant on ionic strength in the presence of ADP was very similar to that in the presence of ATP; it increased about fourfold, from ~1,000 nm 2 /s without KCl to ~3,800 nm 2 /s in the presence of 60 mM KCl (Fig. 1, I–M; and Table I).

Diffusive motility at near-physiological ionic strength is a property of full-length Eg5

Recently, it was shown in optical trapping experiments that a truncated, dimeric human Eg5 motor construct is capable of only very short processive runs (Valentine et al., 2006). No diffusive motility was reported. However, in a similar assay, full-length Eg5 moved processively over longer distances, but in an irregular manner, indicating diffusive periods (Korneev et al., 2007). To explore the motility of single dimeric Eg5 motors under various ionic conditions, we generated a C-terminal GFP fusion with the N-terminal 513 amino acids of *X. laevis* Eg5 based on the dimeric construct of human Eg5 previously reported (Valentine et al., 2006). The bacterial expression of this protein resulted in a mixture of monomeric and dimeric forms (Fig. S1 A, available at <http://www.jcb.org/cgi/content/full/jcb.200801145/DC1>).

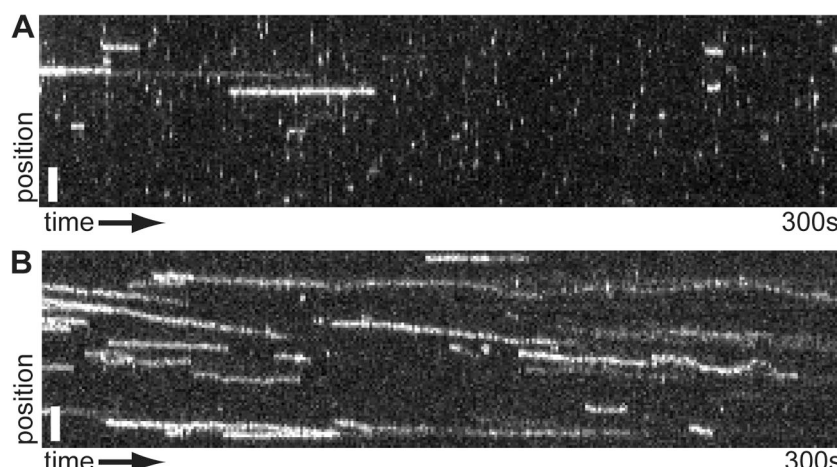


Figure 2. Dimeric Eg5 exhibits persistent microtubule association only at ionic strength well below physiological conditions. (A) Kymograph of the displacement of 230 pM Eg5-513-GFP dimers versus time in 80 mM Pipes buffer with 0.2 mM ATP. A large majority of binding events last two frames or less (<2 s). Similar results were obtained at 2 mM ATP (not depicted). (B) Kymographs showing processive runs by 14 pM Eg5-513-GFP dimers in 20 mM Pipes with 2 mM ATP. Bars, 2 μ m.

Size exclusion chromatography was used to isolate the dimeric form, which was then used in imaging experiments. We confirmed that the purified dimer contains two GFPs under all assayed conditions based on its fluorescent properties (Fig. S1, B–G). Motility assays showed that under high ionic strength conditions, motors only remained microtubule bound for very short periods (<2 s), and motility could not be resolved (Fig. 2 A). To exclude the possibility that this construct was inactive, we tested motility at low ionic strength (20 mM Pipes) and observed persistent directional runs (Fig. 2 B). These data suggest that a homotetramer-specific diffusive mode keeps full-length Eg5 attached to a microtubule for longer times at near physiological conditions. It is also possible that this diffusive mode involves interactions between the C terminus of Eg5 and microtubules, as suggested in microtubule-bundling experiments with *Drosophila melanogaster* kinesin-5 constructs (Tao et al., 2006).

Eg5 moves directionally on microtubule bundles at high ionic strength

We have shown previously that Eg5 can cross-link two microtubules and drive their relative movement by moving toward both plus ends in an ATP-dependent manner even at high ionic strength (Kapitein et al., 2005). This appears to be inconsistent with the diffusive behavior of Eg5-GFP observed here under these conditions. One explanation is that the simultaneous interaction of individual Eg5 tetramers with two microtubules enhances directional motion. To test this, we examined the motion of Eg5-GFP on bundles of microtubules (axonemes), which might allow Eg5 molecules to interact with more than one microtubule at the same time (Fig. 3 A). On axonemes, single Eg5 motors made directional runs of several micrometers (Fig. 3 B), even at salt concentrations (70 mM Pipes plus 60 mM KCl) at which Eg5's motility on single microtubules was purely diffusive (Fig. 1, H–L). MD and MSD analyses indicate that the motility of Eg5 on axonemal microtubule bundles has an ATP-dependent directional component in addition to 1D diffusion, even at a high ionic strength (Fig. 3, C and D). This result is

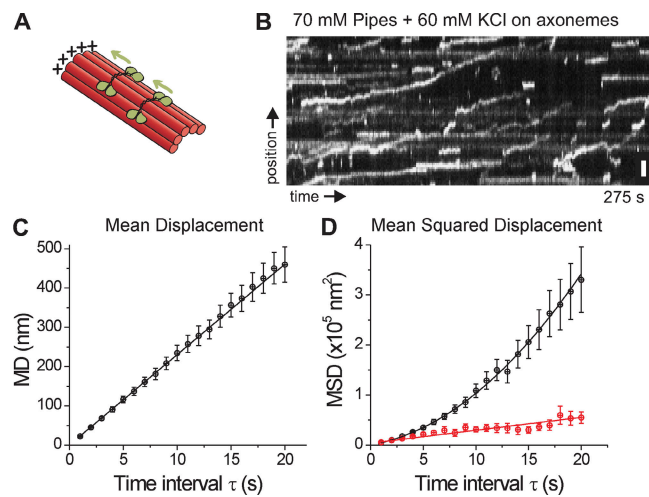


Figure 3. Full-length Eg5 motility at high ionic strength is directional on microtubule bundles (axonemes). (A) Cartoon of a possible interaction geometry of Eg5 with microtubule bundles. Note that Eg5 has a length of ~ 80 nm (Kashina et al., 1996), and an axoneme has a diameter of 200 nm, with microtubule doublets being ~ 70 nm apart (Alberts et al., 2002). (B) Kymographs of Eg5-GFP motility versus time on an axoneme in the presence of ATP. (C) MD calculated from motility recordings in the presence of ATP. Fit represents $MD = v\tau$ ($v = 23$ nm/s). (D) MSD calculated from different motility recordings in the presence of ATP (black) or ADP (red). Fit for ATP represents $MD = \sqrt{v^2 + 2D\tau}$ ($v = 26$ nm/s; $D = 1.8 \times 10^3$ nm 2 /s). Fit for ADP represents $MD = 2D\tau$ ($D = 1.3 \times 10^3$ nm 2 /s). Error bars represent SD. Bar, 1 μ m.

consistent with directionality being caused by the interaction of Eg5 with two microtubules, although we cannot rule out an influence of particular properties of axonemal microtubules.

Eg5 can switch from diffusive to directional motion upon binding a second microtubule

To directly test whether Eg5 motion is regulated through interactions with a second microtubule, we used Eg5-GFP in a microtubule–microtubule sliding assay (Fig. 4 A; Kapitein et al., 2005). Microtubules were immobilized on the glass surface,

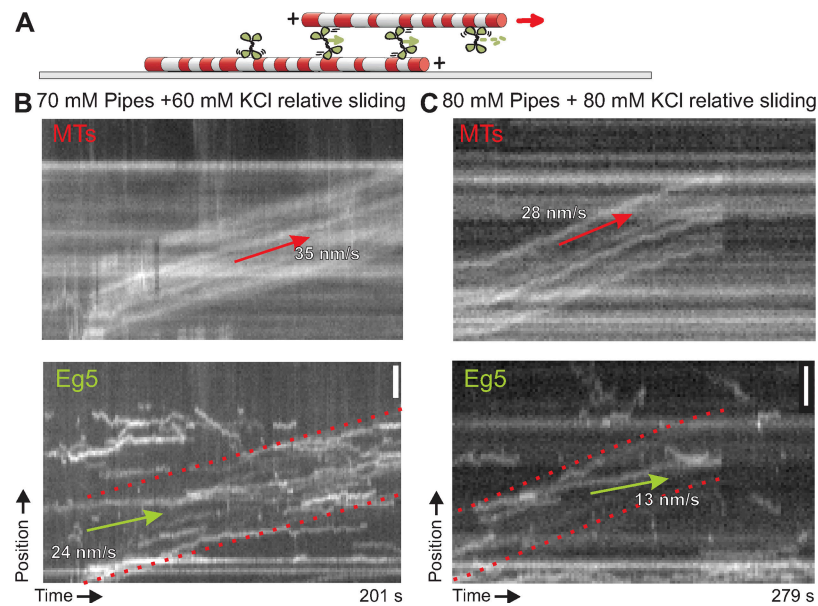


Figure 4. Eg5-GFP-driven relative sliding of microtubules. (A) Cartoon illustrating assay. A sparsely labeled microtubule is surface attached, whereas another microtubule binds with an antiparallel orientation and is moved by Eg5 homotetramers. (B and C) Top kymographs show sliding of a microtubule relative to surface-attached microtubule at 35 (B) and 28 nm/s (C). Below, corresponding kymographs of Eg5-GFP show directional runs (~ 25 [B] and ~ 13 nm/s [C]) between two overlapping microtubules (region marked with two red dotted lines) and diffusive motility in regions without overlap. The slope of the arrows indicate the velocity of motors (green) or microtubules (red). Bars, 2 μ m.

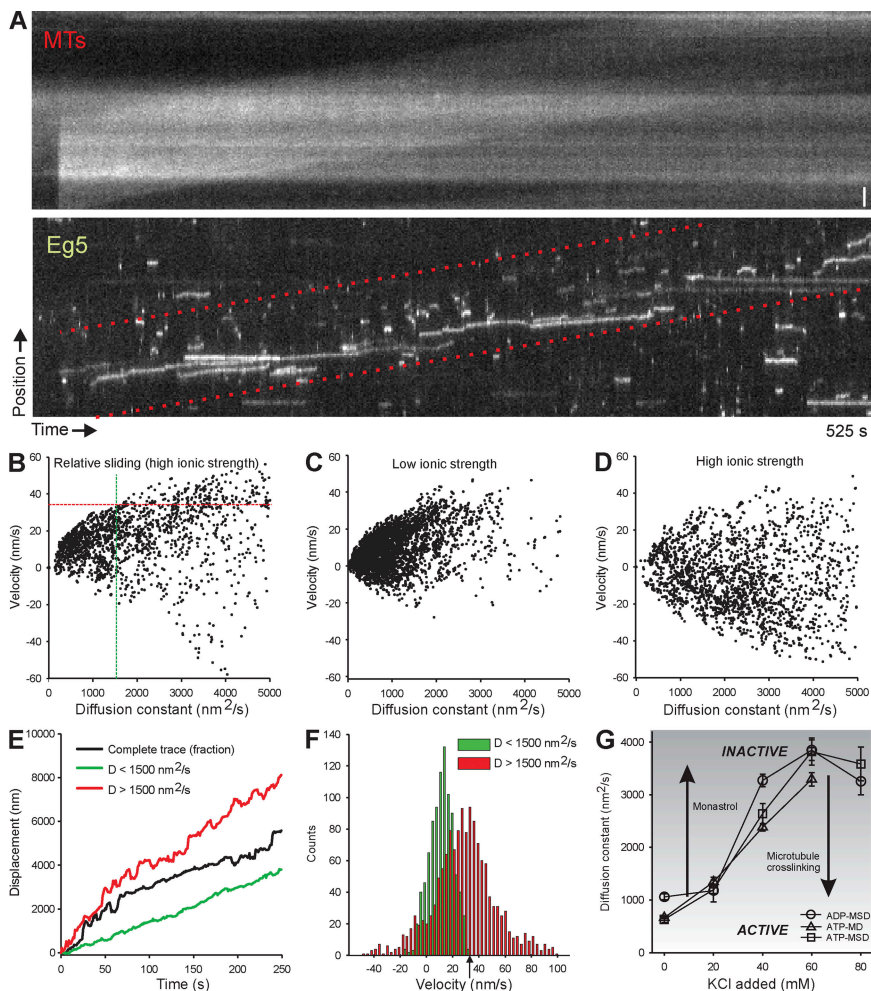


Figure 5. Full-length Eg5-GFP switches from diffusive to directional motility upon binding to a second microtubule. Data collected as described in Fig. 4, but in the presence of a mixture of 1 nM Eg5-GFP and 2 nM of unlabeled tetrameric Eg5. (A) Top kymograph shows sliding of a microtubule (MT) relative to a surface-attached microtubule. Below, the corresponding kymograph of Eg5-GFP shows directional runs between the overlapping microtubules (region marked with two red dotted lines). (B–F) Analysis of Eg5 motility during relative sliding. (B) Scatter plot of all pairs of short-term velocity and diffusion constant determined for a window of 15 s moving over the composite position-time trace of 94 Eg5 motors traced in the overlap zone of 11 microtubule pairs (2,335 points obtained from 2,349 s of total time). The horizontal dotted line indicates the average velocity of sliding microtubules (33 nm/s), and the vertical dotted line indicates the threshold used to discriminate slow and fast diffusion. (C and D) Similar analyses for Eg5 moving on individual microtubules at low ionic strength (C, 70 mM Pipes; Fig. 1; 4,266 points) and high ionic strength (D, data pooled from 70 mM Pipes + 60 mM KCl and 70 mM Pipes + 80 mM KCl; 2,478 points). (E) Position-time traces. Black, fraction of the composite trace used for B. Green and red, sorted time points with a short-term diffusion constant; $D < 1,500 \text{ nm}^2/\text{s}$ (green) and $D > 1,500 \text{ nm}^2/\text{s}$ (red). (F) Histograms of the short-term velocities as obtained from the time points in the green and red trace in E. The arrow indicates the average microtubule sliding velocity. (G) Graph summarizing Eg5 behavior under various conditions. Bar, 2 μm .

and Eg5-GFP was added with additional microtubules in a high ionic strength buffer (70 mM Pipes + 60 mM KCl or 80 mM Pipes + 80 mM KCl). As observed in Fig. 1, Eg5 diffused along individual microtubules without observable bias. Microtubules in solution occasionally became cross-linked by Eg5 to an immobilized microtubule and were moved unidirectionally along the stationary microtubule. Simultaneously imaging the GFP-tagged Eg5 and the fluorescently labeled microtubules allowed us to observe the motility of both the microtubules and the individual motor proteins moving between them. Two examples are shown in Fig. 4 (B and C). In the microtubule overlap region, several motor trajectories with clearly directional character can be distinguished (Fig. 4, B and C; bottom), whereas Eg5 motility on the individual microtubules outside of the overlap region remained diffusive. The velocity of such directional runs in the overlap region was typically lower (~24 nm/s in Fig. 4 B and ~13 nm/s in Fig. 4 C; bottom) than the microtubule gliding speed (35 nm/s in Fig. 4 B and 28 nm/s in Fig. 4 C; top). From seven different recordings of Eg5-GFP-driven relative sliding in which single-motor motility could be discerned, we found the ratio between motor speed and microtubule speed to be 0.6 (± 0.1 [SD]). This directly demonstrates that microtubule gliding is driven by the simultaneous directional movement of Eg5 on both cross-linked antiparallel microtubules resulting in a microtubule gliding speed that is twice the motor speed.

In these experiments, microtubule sliding events with sufficiently sparse motors to map individual trajectories were rare. To overcome this problem, we performed experiments at lower concentrations of Eg5-GFP, but in the presence of unlabeled Eg5 (Fig. 5 A). Trajectories of 94 motors between 11 overlapping and sliding microtubule pairs (mean velocity \pm SD = 33 \pm 6 nm/s) could now be traced. Analysis of motor motility in the overlap region is complicated by not knowing whether motors at any given time interact with just one or with both microtubules. For example, Eg5 molecules that appear to move directionally could actually be freely diffusing on the sliding microtubule, being transported along with it. In addition, motors can switch between modes of interaction. The three possible motor populations can, in principle, be distinguished based on their average speeds and diffusion constants. Motors diffusing on the transported microtubule should exhibit both a high speed and a high diffusion constant, whereas motors driving microtubule sliding are expected to move at half the translocated microtubule's speed with a lower diffusion constant.

To distinguish, without bias, intervals corresponding to active, directional motility from passive diffusion (along either the immobile or the sliding microtubule), we calculated the MSD and MD over 15-s intervals to obtain short-term diffusion constants and velocities (Douglass and Vale, 2005). Fig. 5 (B–D) shows scatter plots of the short-term velocity versus short-term

diffusion constant for Eg5 in between sliding microtubules at high ionic strength (Fig. 5 B), Eg5 on individual microtubules (Fig. 1) at low ionic strength (70 mM Pipes; Fig. 5 C), and high ionic strength (70 mM Pipes + 60/80 mM KCl; Fig. 5 D). These data reveal that Eg5 motility between sliding microtubules is a mixture of the two types of motility observed on single microtubules at low and high ionic strength (directional and non-directional; diffusive). We next sorted all time points into two categories: one corresponding to all time points with a short-term diffusion constant $<1,500 \text{ nm}^2/\text{s}$, and the second one corresponding to diffusion constants $>1,500 \text{ nm}^2/\text{s}$ (Fig. 5, B and E). The velocity distribution of the first class ($D < 1,500 \text{ nm}^2/\text{s}$; Fig. 5 F) is narrow and peaks around 15 nm/s (mean velocity $\pm \text{SD} = 12 \pm 8 \text{ nm/s}$). The velocity distribution of the second class ($D > 1,500 \text{ nm}^2/\text{s}$) is much wider and peaks around 30 nm/s, similar to the velocity of sliding microtubules.

From this analysis, we conclude that, for individual Eg5 tetramers in the overlap zone of two sliding microtubules, there is a strong correlation between the diffusion constant and the velocity. Some of the motors move for part of the time with a velocity of $\sim 15 \text{ nm/s}$ and with a relatively low diffusion constant, which is analogous to Eg5-GFP's motility along single microtubules at low salt concentrations (Fig. 1). A second class has a higher diffusion constant and a velocity corresponding to that of the sliding microtubule. This second class consists of motors that are (occasionally) diffusing on the sliding microtubule and get transported with it. Collectively, these results demonstrate that Eg5 can switch from diffusive motility to directional motility upon binding to a second microtubule (Fig. 5 G).

Potential regulatory mechanisms for homotetrameric Eg5

We have shown that full-length Eg5's motility comprises an unbiased, diffusive mode independent of ATP hydrolysis and a plus end-directed processive mode that requires ATP hydrolysis. The balance of these modes depends on ionic strength, cross-link geometry, and, as we have shown previously, monastrol concentration (Fig. 5 G; Kwok et al., 2006). At high ionic strengths, full-length Eg5's motility on single microtubules is predominantly diffusive, whereas dimeric Eg5 associates only very briefly, suggesting that domains (motor or nonmotor) in the full-length homotetramer contribute to the interaction that mediates diffusion. Decreasing the ionic strength enhances the directionality of full-length Eg5 and increases the processive run length of dimers. The run length of a processive motor is determined by the ability to keep the nucleotide states of its two motor domains out of phase. Runs terminate when both domains are in the ADP-bound state. We speculate that with ADP on all heads, dimeric Eg5 detaches from the microtubule, whereas full-length Eg5 enters its diffusive mode. For full-length Eg5, the similar effect of monastrol and increasing salt can be understood if both inhibit ADP release, thereby promoting an ADP-ADP diffusive state. Indeed, kinetic studies on Eg5 inhibition indicate that monastrol stabilizes the ADP-bound state (DeBonis et al., 2003; Cochran et al., 2005). In addition, a strong decrease in microtubule-stimulated ATPase activity at increased ionic

strength has been reported for a monomeric construct of human Eg5 (DeBonis et al., 2003).

We have also demonstrated that homotetrameric Eg5's binding to a second microtubule alters the balance between diffusive and directional motion. The question remains how a signal affecting mechanochemistry gets transmitted from one end of the homotetrameric molecule to the other end. Electron micrographs of Eg5 show very straight conformations of the stalk, without evidence for hinges (Kashina et al., 1996). It is thus unlikely that Eg5's regulation uses a large-scale hinge motion. This would be in contrast to kinesin-1, in which the cargo-inhibited folding of the tail onto the motor domains turns off the motor (Friedman and Vale, 1999; Stock et al., 1999). On the other hand, the tail domain of the opposing dimer of Eg5 is likely located close to where the folded tail domain of a kinesin-1 dimer would be in the inhibited state. It could thus play a regulatory role with only relatively small conformational changes. Another possibility is that changes in thermal motions of the distal motor domains are coupled to fluctuations in the stalk, which, in turn, control the balance between diffusive modes and processive bursts in the proximal motor domains. Such a mechanism has been hypothesized for molecular motors such as dynein (Bray and Duke, 2004; Hawkins and McLeish, 2006). Further experimental work, possibly using optical traps to apply well-controlled loads, will be needed to explore how a mechanical signal on one end of the molecule can switch the motility of homotetrameric Eg5.

In summary, our results provide evidence for a functional specialization of Eg5 that is thus far unique among the kinesins, namely the capability to switch between different modes of motion on microtubules in response to binding another microtubule. Our data suggest that ATP-dependent directional motility is suppressed when Eg5 interacts with only one microtubule and is activated upon binding a second microtubule. This could equip a homotetrameric kinesin with cargo sensitivity and increase its energy efficiency. In addition, nonspecific attachment to and ATP-independent diffusion along single microtubules enhances the probability of capturing another microtubule. After cross-linking, Eg5 switches to directional motility and drives the sorting of these microtubules. These findings provide an important step toward understanding the complex regulation of Eg5 and its contribution to bipolar spindle assembly during cell division.

Materials and methods

Protein constructs

A recombinant full-length *X. laevis* Eg5-GFP construct was expressed and purified as described previously (Kwok et al., 2006). To generate dimeric GFP-labeled Eg5, a fragment of the *X. laevis* Eg5 gene coding for the N-terminal 513 amino acids was amplified by PCR, fused in frame to GFP, and inserted into the bacterial expression vector pRESET. The linker sequence GSSGGGGSGGGGGSGGGGS was inserted between Eg5 and GFP, and a tobacco etch virus protease-cleavable polyhistidine tag was added to the C terminus. Eg5-513-GFP was expressed in BL21 *Escherichia coli* and purified as described for the full-length Eg5-GFP with the following modifications (Kwok et al., 2006). Removal of the polyhistidine tag by tobacco etch virus protease was performed at 4°C for 12 h. Purification by size exclusion chromatography was performed with a Superdex-200 column (GE Healthcare). Axonemes (from sea urchin sperm) and Cy5-labeled tubulin (from porcine brain) were prepared according to published procedures (Gibbons and Fronk, 1979; Hyman, 1991; Kapitein et al., 2005).

Motility assays

Single-molecule experiments on full-length Eg5-GFP were performed at 21°C using a previously described custom-built wide-field fluorescence microscope (100x NA 1.3 S-Fluor objective; Nikon; Kapitein et al., 2005), but modified for GFP detection by the addition of a 488-nm excitation laser (Sapphire 488-20; Coherent) and appropriate filters (dichroic mirror Z488RDC/532/633RPC and bandpass filter HQ525/50M; Chroma Technology Corp.). For simultaneous observation of GFP and Cy5, emission light was first filtered with a triple bandpass filter (Z488/532/633M; Chroma Technology Corp.), separated with a dichroic beam splitter (565DCXR; Chroma Technology Corp.), and finally redirected onto the tube lens at slightly different angles, resulting in two separate images on the camera chip (Micromax; Roper Scientific). Data were taken with continuous excitation (20–30 W/cm²) and a 1-s integration time, unless stated otherwise. Experiments with mixtures of Eg5-GFP and wild-type Eg5 (Fig. 5) were performed on a total internal reflection fluorescence (TIRF) microscope (Eclipse TE2000E; Nikon) with a 100x NA 1.49 plan Apo objective, which was described previously (Grigoriev et al., 2008), with the following modifications. The additional 2.5x magnification lens was removed. An image splitter (DualView; Optical Insight) was used to separate Cy5 and GFP emission. The GFP channel was further filtered using a bandpass filter (ET525/50M; Chroma Technology Corp.). An EM CCD camera (QuantEM; Roper Scientific) was used for detection.

Single-molecule motility and photobleaching experiments involving the shorter Eg5-513-GFP construct were performed on another instrument, which was also described previously (Kwok et al., 2006), with the following modifications. The inverted microscope (Axiovert; Carl Zeiss, Inc.) was equipped with a laser TIRF slider (Carl Zeiss, Inc.), a 100x NA 1.45 Alpha Plan-Fluar objective (Carl Zeiss, Inc.), and an EM CCD camera (iXon DU-897; Andor Technology). Data were taken with TIRF illumination from a 491-nm laser source (Cobalt Calypso 50; Solamere Technology) with a 0.4-s exposure time at a frame rate of 1 s⁻¹.

Coverslips were cleaned by ultrasonication in ~0.2 M potassium hydroxide followed by three rounds of ultrasonication in ultrapure water. Coverslips were rendered positively charged by aminosilanization with 3-[2-[2-aminoethylamino]ethylamino]propyl-trimethoxysilane (DETA; Sigma-Aldrich). In some experiments, coating with poly-lysine (Sigma-Aldrich) was used for the same purpose. Sample chambers were first incubated with Cy5-labeled microtubules (in some experiments, rhodamine-labeled microtubules were used; Fig. 5 A) or axonemes for 10 min followed by 5–10-min incubation with 0.2 mg/ml casein. Finally, chambers were perfused with ~100–300 pM of motors in motility buffer. For relative sliding experiments, free microtubules were added to the motility buffer, and the motor concentration was increased three to five times using Eg5-GFP (Fig. 4) or a mixture of 1 nM Eg5-GFP and 2 nM of unlabeled full-length Eg5 (Fig. 5) to enhance landing rates of microtubules.

Motility buffer

Pipes was used as buffering agent. This buffer has two acid groups, and buffering at the pKa (6.8) requires an equimolar amount of HPipes⁻ and Pipes²⁻. Buffering 70 mM of the acid form of Pipes (H₂Pipes) requires the addition of 105 mM KOH, whereas buffering the basic form (K₂Pipes) requires the addition of 35 mM HCl. In the latter case, however, 140 mM K⁺ are contributed by the buffer. The lowest concentration of Pipes used was 70 mM because the buffering capacity at lower concentrations was not sufficient to maintain a constant pH after adding the various other components (Eg5-GFP, ATP, etc.). Consistently, experiments performed with K₂Pipes buffer [70 mM K₂Pipes; 140 mM K⁺ in total] yielded results similar to those made with H₂Pipes in the presence of an additional 60/80 mM KCl (Fig. 5). In addition to the variable amount of KCl, the motility buffers contained 1 mM EGTA, 3 mM MgCl₂, 2 mM ATP or ADP, 14 mM DTT, 10 μM paclitaxel, 25 mM glucose, 20 μg/ml glucose oxidase, and 35 μg/ml catalase.

Data analysis

Motility data were acquired using Winview (Roper Scientific) or MetaMorph (MDS Analytical Technologies) and were analyzed with custom-written routines in LabVIEW (National Instruments). The x-y coordinates of moving fluorescence spots were determined by fitting a 2D Gaussian to the observed intensity profile in each frame. Mainly noncrossing trajectories were analyzed; occasionally a trajectory was traced until it crossed another trajectory. Spots with an intensity four times larger than the average were excluded as well as trajectories shorter than four frames or immobile for more than three frames. The microtubule position was determined from fitting a straight line to all of the motor coordinates of a run. The motor coordinates were then transformed into coordinates along and perpendicular to the microtubule by projection.

Diffusion constant and speed were determined from the MSD as described previously (Kwok et al., 2006). The MSD for purely diffusive motion is a straight line, reflecting the linear increase in positional variance typical for diffusive motion ($MSD = 2 D\tau$). In the case of a directional bias, the MSD will show an additional quadratic component proportional to the velocity (thus, $MSD = 2 D\tau + v^2\tau^2$). Velocity and diffusion constants were also determined from the MDs using the relations $MD = v\tau$ and variance of the MD = $2D\tau$. MDs were calculated in the same way, but without the squaring of displacements. For the calculation of D from the variance of the MD, the standard error of the variance was used as error bars (Taylor, 1997).

In contrast to the MSD calculations, the MD calculations require knowledge of the polarity of the microtubules because in an average over randomly oriented microtubules, the MD would always average to zero. In most experiments, the orientation of the microtubules could be inferred from the overall direction of motion of the motors. In the experiments at high ionic strengths, there was no obvious overall direction of motion, but the orientation of about half of the microtubules could be inferred from a few clearly aggregated clumps of motor (high fluorescence intensity) that still moved directionally (~4% of total events; intensity at least four times that of single motors).

For calculation of the short-term MSD and MD in Fig. 5, traces were merged into one array, and the MSD and MD were calculated for a sliding subarray of size 15 (Douglass and Vale, 2005). D and v were then obtained from a linear fit to the first three points of the MSD ($MSD = 2 D\tau$) and MD ($MD = v\tau$) traces, respectively (excluding zero). For Fig. 5 (E and F), D - v pairs were sorted based on D to yield a distribution of velocities for $D > 1,500 \text{ nm}^2/\text{s}$ [Fig. 5 E] and $D < 1,500 \text{ nm}^2/\text{s}$ [Fig. 5 F]. The same analysis for trajectories on individual microtubules (Fig. 5, C and D) classified 20% of data points above 1,500 nm²/s at low ionic strength and 25% below this cut-off at high ionic strength. The average velocity of high D data points in Fig. 5 C is 16 nm/s. The average velocity of the low D data points in Fig. 5 D is 0.75 nm/s.

Online supplemental material

Fig. S1 shows biochemical and fluorescence characterization of Eg5-513-GFP. Online supplemental material is available at <http://www.jcb.org/cgi/content/full/jcb.200801145/DC1>.

We thank Stefan Lakämper for preparing Cy5-tubulin, Joost van Mameren for writing the kymography and tracking software, and Casper Hoogenraad for use of his equipment.

This project was supported by a research grant from the Human Frontier Science Program (to C.F. Schmidt and T.M. Kapoor) and by the Foundation for Fundamental Research on Matter. L.C. Kapitein and E.J.G. Peterman were supported by a Vidi fellowship to E.J.G. Peterman from the Research Council for Earth and Life Sciences. T.M. Kapoor is grateful to the National Institutes of Health/National Institute of General Medical Sciences for support (grant GM65933). B.H. Kwok was a Merck postdoctoral fellow. J.S. Weinger was supported by training grant to the Rockefeller University (T32 CA009673). Additional support was provided to L.C. Kapitein by the Erasmus Medical Center fellowship program and to C.F. Schmidt by the DFG Research Center Molecular Physiology of the Brain.

Submitted: 23 January 2008

Accepted: 14 July 2008

References

- Alberts, B., A. Johnson, J. Lewis, M. Raff, K. Roberts, and P. Walter. 2002. Molecular Biology of the Cell. Fourth edition. Garland Science, New York. 1548 pp.
- Bray, D., and T. Duke. 2004. Conformational spread: the propagation of allosteric states in large multiprotein complexes. *Annu. Rev. Biophys. Biomol. Struct.* 33:53–73.
- Cochran, J.C., J.E. Gatial, T.M. Kapoor, and S.P. Gilbert. 2005. Monastrol inhibition of the mitotic kinesin Eg5. *J. Biol. Chem.* 280:12658–12667.
- Cole, D.G., W.M. Saxton, K.B. Sheehan, and J.M. Scholey. 1994. A slow homotetrameric kinesin-related motor protein purified from *Drosophila* embryos. *J. Biol. Chem.* 269:22913–22916.
- Culver-Hanlon, T.L., S.A. Lex, A.D. Stephens, N.J. Quintyne, and S.J. King. 2006. A microtubule-binding domain in dynein increases dynein processivity by skating along microtubules. *Nat. Cell Biol.* 8:264–270.
- DeBonis, S., J.P. Simorre, I. Crevel, L. Lebeau, D.A. Skoufias, A. Blangy, C. Ebel, P. Gans, R. Cross, D.D. Hackney, et al. 2003. Interaction of the mitotic inhibitor monastrol with human kinesin Eg5. *Biochemistry*. 42:338–349.

Douglass, A.D., and R.D. Vale. 2005. Single-molecule microscopy reveals plasma membrane microdomains created by protein-protein networks that exclude or trap signaling molecules in T cells. *Cell*. 121:937–950.

Friedman, D.S., and R.D. Vale. 1999. Single-molecule analysis of kinesin motility reveals regulation by the cargo-binding tail domain. *Nat. Cell Biol.* 1:293–297.

Gibbons, I.R., and E. Fronk. 1979. Latent adenosine-triphosphatase form of Dynein-1 from sea urchin sperm flagella. *J. Biol. Chem.* 254:187–196.

Grigoriev, I., S. Gouveia, B. Van der Vaart, J. Demmers, J.T. Smyth, S. Honnappa, D. Splinter, M.O. Steinmetz, J.W. Putney, C.C. Hoogenraad, and A. Akhmanova. 2008. STIM1 is a MT-plus-end-tracking protein involved in remodeling of the ER. *Curr. Biol.* 18:177–182.

Hackney, D.D., J.D. Levitt, and J. Suhan. 1992. Kinesin undergoes a 9-S to 6-S conformational transition. *J. Biol. Chem.* 267:8696–8701.

Hawkins, R.J., and T.C.B. McLeish. 2006. Dynamic allostery of protein alpha helical coiled-coils. *J. R. Soc. Interface*. 3:125–138.

Helenius, J., G. Brouhard, Y. Kalaidzidis, S. Diez, and J. Howard. 2006. The depolymerizing kinesin MCAK uses lattice diffusion to rapidly target microtubule ends. *Nature*. 441:115–119.

Hildebrandt, E.R., L. Gheber, T.J. Kingsbury, and M.A. Hoyt. 2006. Homotetrameric form of CIN8P, an *S. cerevisiae* kinesin-5 motor, is essential for its in vivo function. *J. Biol. Chem.* 281:26004–26013.

Hyman, A.A. 1991. Preparation of marked microtubules for the assay of the polarity of microtubule-based motors by fluorescence. *J. Cell Sci. Suppl.* 14:125–127.

Kapitein, L.C., E.J. Peterman, B.H. Kwok, J.H. Kim, T.M. Kapoor, and C.F. Schmidt. 2005. The bipolar mitotic kinesin Eg5 moves on both microtubules that it crosslinks. *Nature*. 435:114–118.

Kashina, A.S., R.J. Baskin, D.G. Cole, K.P. Wedaman, W.M. Saxton, and J.M. Scholey. 1996. A bipolar kinesin. *Nature*. 379:270–272.

Korneev, M.J., S. Lakamper, and C.F. Schmidt. 2007. Load-dependent release limits the processive stepping of the tetrameric Eg5 motor. *Eur. Biophys. J.* 36:675–681.

Kuznetsov, S.A., and V.I. Gelfand. 1986. Bovine brain kinesin is a microtubule-activated ATPase. *Proc. Natl. Acad. Sci. USA*. 83:8530–8534.

Kwok, B.H., L.C. Kapitein, J.H. Kim, E.J.G. Peterman, C.F. Schmidt, and T.M. Kapoor. 2006. Allosteric inhibition of kinesin-5 modulates its processive directional motility. *Nat. Chem. Biol.* 2:480–485.

Okada, Y., and N. Hirokawa. 2000. Mechanism of the single-headed processivity: diffusional anchoring between the K-loop of kinesin and the C terminus of tubulin. *Proc. Natl. Acad. Sci. USA*. 97:640–645.

Sawin, K.E., K. Leguellec, M. Philippe, and T.J. Mitchison. 1992. Mitotic spindle organization by a plus-end-directed microtubule motor. *Nature*. 359:540–543.

Sharp, D.J., G.C. Rogers, and J.M. Scholey. 2000. Microtubule motors in mitosis. *Nature*. 407:41–47.

Stock, M.F., J. Guerrero, B. Cobb, C.T. Eggers, T.G. Huang, X. Li, and D.D. Hackney. 1999. Formation of the compact conformer of kinesin requires a COOH-terminal heavy chain domain and inhibits microtubule-stimulated ATPase activity. *J. Biol. Chem.* 274:14617–14623.

Tao, L., A. Mogilner, G. Civelekoglu-Scholey, R. Wollman, J. Evans, H. Stahlberg, and J.M. Scholey. 2006. A homotetrameric kinesin-5, KLP61F, bundles microtubules and antagonizes Ncd in motility assays. *Curr. Biol.* 16:2293–2302.

Taylor, J.R. 1997. An introduction to error analysis: the study of uncertainties in physical measurements. Second edition. University Science Books, Sausalito, CA. 327 pp.

Vale, R.D., D.R. Soll, and I.R. Gibbons. 1989. One-dimensional diffusion of microtubules bound to flagellar dynein. *Cell*. 59:915–925.

Valentine, M.T., P.M. Fordyce, T.C. Krzysiak, S.P. Gilbert, and S.M. Block. 2006. Individual dimers of the mitotic kinesin motor Eg5 step processively and support substantial loads in vitro. *Nat. Cell Biol.* 8:470–476.

Wittmann, T., A. Hyman, and A. Desai. 2001. The spindle: a dynamic assembly of microtubules and motors. *Nat. Cell Biol.* 3:E28–E34.